XII International Conference on Computational Plasticity. Fundamentals and Applications
COMPLAS XII
E. Oñate, D.R.J. Owen, D. Peric and B. Suárez (Eds)

NUMERICAL SIMULATION BASED ON FEM / MLS COUPLING FOR SOLID MECHANICS

Y. GHOZZI[*], C. LABERGERE[*] AND P. VILLON [†]

[*] ICD/LASMIS, STMR UMR-CNRS 6279
University of Technology of Troyes, France
Email: yosr.ghozzi@utt.fr, carl.labergere@utt.fr

[†] Roberval, UMR 6253
University of Technology of Compiegne, France
Email: pierre.villon@utc.fr

Key words: MLS, coupled FEM/MLS, interpolant weight functions, nodal integration.

Abstract. This paper presents the development of Meshless Methods based on the weighted least squares approximation (MLS) [1,3,14] to solve 2D mechanical problems. A particular construction support of weight functions involved in the construction of the MLS shape functions is elaborated. We propose a numerical simulation based on the coupling between the FEM and the MLS method. A Huerta et al. formulation is used to build the MLS shape function in the transition area FEM/MLS.

1 INTRODUCTION

Meshless methods have been proposed to deal with some numerical problems for solid mechanics such as large deformations, occurrence of high stress gradient or singularities and mechanical fields' discontinuities. However, these methods are not easy to implement and shape functions are generated by iteration process [1]. In this paper, MLS approximation for a 2D problem is developed. The influence of different weight functions on numerical implementation response, especially for weight interpolating functions [4,10,13] is studied. A new smooth support C^1 weight function is proposed to manage some numerical integration problems. On the other hand, a method of nodal integration regularized gradient [5] was developed, to deal with rational functions integration problems. For Finite Element Method (FEM) and MLS method coupling [2], a 2^{nd} order polynomial consistency was satisfied. Galerkin variational form is used to solve equilibrium [1,6]. A tensile test example of a 2D plane specimen with nonlinear elastoplasticity model and small perturbations is simulated with Abaqus® software and compared with our own software of FEM /MLS coupling.

2 MOVING LEAST SQUARE APPROXIMATION (MLSA)

For an available meshless approximation scheme, the moving least square (MLS) is considered to approximate random data from a discrete solution. Approximate function and gradient continuity are assumed. For a 2D problem, we consider $\underline{p}$ a polynomial basis, with m is the basis dimension. The linear basis is $\underline{p}^T = \langle 1, x, y \rangle$ (m=3) and the quadratic one is

$\underline{p}^T = \langle 1, x, y, \frac{x^2}{2}, xy, \frac{y^2}{2} \rangle$ (m=6). Considering a 2D sub-domain Ω we approximate the distribution of the vector displacement $\underline{u}^T = \langle u_x, u_y \rangle$ in the domain, over a number of randomly located nodes $\underline{x}_i^T = \langle x_i, y_i \rangle$, i=1, 2,…, n_{tot}. The MLS approximation $u_x^h(\underline{x})$ of $u_x, \forall x, y \in \Omega$, can be written as:

$$u_x^h(\underline{x}) = \underline{p}^T(\underline{x}).\underline{a}(\underline{x}) \tag{1}$$

Considering y an evaluation point different from MLS nodes for an approximation centered scheme.

$$\underline{p}^T(\underline{y}) \,.\underline{a}(\underline{x}) = \underline{p}^T(\underline{y} - \underline{x}).\underline{a}(\underline{x}) \tag{2}$$

The approximant MLS $u_x^h(\underline{x})$ of u_x $\forall x, y \in \Omega$ is expressed as follow:

$$u_x^h(\underline{x}) = \underline{p}^T(\underline{0}).\underline{a}(\underline{x}) \tag{3}$$

The coefficient vector $\underline{a}(\underline{x})$ is resolved by minimizing a weighted discrete L_2 norm defined as:

$$J(\underline{x}) = \sum_{I=1}^{n_{loc}} w(\underline{x}_I, \underline{x}) \,[\underline{p}(\underline{x}_I - \underline{x}).\underline{a}(\underline{x}) - \hat{\underline{u}}_I]^2 = [\,\underline{\underline{P}}.\underline{a}(\underline{x}) - \hat{\underline{u}}]^T \underline{\underline{W}} \,[\,\underline{\underline{P}}.\underline{a}(\underline{x}) - \hat{\underline{u}}] \tag{4}$$

Where $w(\underline{x}_I, \underline{x})$ the weight function associated to the node *I*, n_{loc} the number of nodes MLS *"I"* for which $w(\underline{x}_I, \underline{x}) \neq 0$, $\hat{\underline{u}}_I$ are the nodal displacement of a node *I* along x direction, the matrix $\underline{\underline{P}}$ and $\underline{\underline{W}}$ are defined as:

$$\underline{\underline{P}} = \begin{bmatrix} \underline{p}^T(\underline{x}_1 - \underline{x}) \\ \underline{p}^T(\underline{x}_2 - \underline{x}) \\ \cdot \\ \cdot \\ \cdot \\ \underline{p}^T(\underline{x}_{n_{loc}} - \underline{x}) \end{bmatrix}_{n_{loc} * m} \quad , \quad \underline{\underline{W}}(\underline{x}) = \begin{bmatrix} w(\underline{x}_I, \underline{x}) \ldots 0 \\ \ldots \ \ldots \ \ldots \\ 0 \quad \ldots \ w(\underline{x}_I, \underline{x}) \end{bmatrix}_{n_{loc} * n_{loc}} \quad , \quad \hat{\underline{u}}^T = [\hat{\underline{u}}_1 \,,\ \hat{\underline{u}}_2 \,, \ldots, \hat{\underline{u}}_n]$$

Eq. (4) leads to the subsequent linear relation between $\underline{a}(\underline{x})$ and $\hat{\underline{u}}$:

$$\underline{\underline{A}}(\underline{x}).\underline{a}(\underline{x}) = \underline{p}(\underline{0}) \tag{5.a}$$

$$\underline{\underline{A}}(\underline{x}) = \underline{\underline{P}}^T \underline{\underline{W}} \,\underline{\underline{P}} = \sum_{I=1}^{n_{loc}} w(\underline{x}_I, \underline{x}) \underline{p}(\underline{x}_I - \underline{x}) \,\underline{p}^T(\underline{x}_I - \underline{x}) \tag{5.b}$$

The MLS approximation is defined when the matrix $\underline{\underline{A}}(\underline{x})$ is non-singular if $\underline{\underline{P}}$ rank is equal to m and regular if $n_{loc} \geq$m. However, if the support is wide on a number of rather important nodes n, we lose the local interpolation character.

By solving Eq. (5.a) and substituting $\underline{a}(\underline{x})$ into Eq. (3) we obtain the following expression of the shape function:

$$u_x^h(\underline{x}) = \sum_{I=1}^{n_{loc}} \phi_I^{MLS}(\underline{x}) \,\hat{u}_{xI} \text{ avec } \phi_I^{MLS}(\underline{x}) = w(\underline{x}_I, \underline{x}) \underline{p}^T(\underline{x}_I - \underline{x}) \underline{a}(\underline{x}) \tag{6}$$

Where $\phi_I^{MLS}(\underline{x})$ is the shape function of the MLS Approximation corresponding to a nodal point $\underline{x}_I$. $\phi_I^{MLS}(\underline{x}) = 0$ when $w(\underline{x}_I, \underline{x}) = 0$ (see Eq.6); thus the similarity of the support of both functions conserves the local character of the MLS approximation. We note that if

$w(\underline{x}_I, \underline{x}) \in C^k(\Omega)$ and $\underline{p}_j(\underline{x}) \in C^l(\Omega)$, $I=1,2,..,n_{loc}$, $j=1, 2,..,m$; then $\phi_I^{MLS}(\underline{x}) \in C^r(\Omega)$ where $r=min(k,l)$. This work is available for nodal displacement $\hat{u}_{yi}$ along y direction since $\underline{u}^T = \langle u_x, u_y \rangle$.

3 WEIGHT FUNCTION

Consider the decomposition of domain $\Omega = \sum_{i=1}^{p} \Omega_i^I$ based on set of MLS nodes. Each node affects the built of the shape functions associated with its neighborhood or domain of influence which can be of any shape: square, circular, etc. In this paper we propose a 2-dimensional boundary line, built with Ω_i^I sub-domains, as a support of the weight function. Each support granted to each node MLS (here node $\underline{x}_i$) is built by sweeping starting from a point $\underline{x}_c$ on the support (Fig.1.c). The computing of the weight function for a point M is ensured by the fraction s like follow:

$$w(\underline{x}_i, \underline{x}) = \begin{cases} w_p\left(\dfrac{\|\underline{x}_i - \underline{x}\|}{r_i}\right) & circulaire \\ w_p\left(\dfrac{|(\underline{x}_i - \underline{x}).\vec{x}|}{a_i}\right) w_p\left(\dfrac{|(\underline{x}_i - \underline{x}).\vec{y}|}{b_i}\right) & rectangular \\ w_p\left(\dfrac{\|\underline{x}_i - \underline{x}\|}{\|\underline{x}_c - \underline{x}\|}\right) & polygonal \end{cases} \quad (7)$$

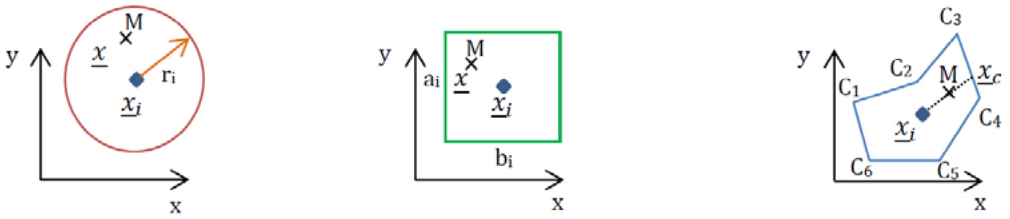

Figure 1: Weight function support definition a) circular support, b) rectangular support, c) polygonal support

A smoothing of the polygon's corners was carried out by a Bezier curves so as to guarantee at least a C^1 continuity. The construction of a Bezier curve (Fig.2) is carried out by respecting the tangency character on A_0 and A_2 and fixing their position with the radius curve θ (Eq.8.a).

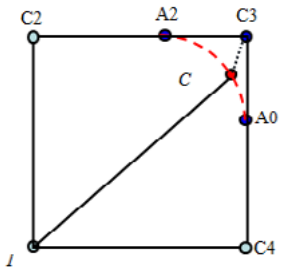

Figure 2: Smooth support construction - Bezier curve

$$\begin{aligned} \overrightarrow{C_4A_0} &= (1-\theta)\overrightarrow{C_4C_3} \\ \overrightarrow{C_2A_2} &= (1-\theta)\overrightarrow{C_2C_3} \end{aligned} \quad (8.a)$$

Then, a spline tangent is built with C_4A_0 and C_2A_2, which leads to the curve construction as below in Eq.8.b.

$$\overrightarrow{IC} = (1-t^2)\overrightarrow{IA_0} + 2*t(1-t)\overrightarrow{IC_3} + t^2\overrightarrow{IA_2} \tag{8.b}$$

In implementing the MLS approximation, the basis function and weight functions should be selected at first. Weight function $w(\underline{x}_i, \underline{x})$ is strictly positive in a sub-domain containing $\underline{x}_i$ and zero outside what is called the support of influence of $\underline{x}_i$. Both Gaussian and spline weight functions with compact supports have been developed. But in the present paper, the cubic spline weight functions were chosen to assume some integration difficulties (see [3]). Weight functions were considered as follow:

$$w_p(s) = 1 - 6s^2 + 8s^3 - 3s^4 \tag{9}$$

To avoid the strong dependence of shape functions to the domain of influence caused by MLS approximation approach, a regularized weight functions were proposed (see [4, 10, 14]). Considering $\sum_{i=1}^{n} w(\underline{x}_i, \underline{x}) = 1$, we build singular weight functions satisfying the following condition:

$$w^a(\underline{x}_i, \underline{x}) = w(\underline{x}_i, \underline{x})/(1 - w(\underline{x}_i, \underline{x})) \text{ , i=1, 2,…,n, here } w^a(|\underline{x}_i - \underline{x}|) \to \infty \; if \; \underline{x} \to \underline{x}_i \tag{10.a}$$

To fulfill MLS interpolation condition ($\phi_i^{MLS}(\underline{x}) \approx \delta_{ij}$) with high accuracy the expression of interpolated weight function w_i^b of a node i at an interpolant point x is as follow:

$$w^b(\underline{x}_i, \underline{x}) = w^a(\underline{x}_i, \underline{x})/\sum_{j=1}^{n} w^a(\underline{x}_j, \underline{x}) \text{ , i=1, 2,…,n, here } w^b(|\underline{x}_i - \underline{x}|) \to \infty \; if \; \underline{x} \to \underline{x}_i \tag{10.b}$$

4 COUPLED FEM/MLS

4.1 Consistency

Consider a set of nodes $\underline{x}_i$ in $\Omega = \Omega^{FEM} \cup \Omega^{MLS} \cup \Omega^{FEM/MLS} / \Omega \subset \Re^n$ which $\Omega^{FEM/MLS}$ is the transition zone between MLS and FEM shape functions (Fig.3). The MLS method is based on an approximation where the shape functions do not satisfy the Kronecker condition. Therefore, Huerta et al [9] proposed a combination of MLS and finite elements in the transition zone (Eq.11) ensuring a consistency condition (Eq.12) (see [2,6, 8,9,10]).

$$\forall \underline{x} \in \Omega^{FEM/MLS} \qquad u_x^h(\underline{x}) = \sum_{j \in \Omega^{FEM/MLS}} N_j^e(\underline{x}) \hat{\underline{u}}_{xj}^{FEM} + \sum_{i \in \Omega^{MLS} \cup \Omega^{FEM/MLS}} \phi_i^{MLS}(\underline{x}) \hat{\underline{u}}_{xi}^{MLS} \tag{11}$$

$\forall \underline{x} \in \Omega^{FEM/MLS}$, $N_j^e(\underline{x})$ and $\phi_i^{MLS}(\underline{x})$ are MLS and FEM shape functions respectively, $\hat{\underline{U}}_{xi}$ and $\hat{\underline{U}}_{xj}$ are their nodal values. In the case of a centered scheme, the consistency condition is expressed bellow:

$$\underline{p}(\underline{0}) = \sum_{je\,\Omega^{FEM/MLS}} N_j^e(\underline{x}) \underline{p}(\underline{x}_j - \underline{x}) + \sum_{ie\,\Omega^{MLS} \cup \Omega^{FEM/MLS}} \phi_i^{MLS}(\underline{x}) \underline{p}(\underline{x}_i - \underline{x}) \tag{12}$$

This coupling changes the equation 5.a as follow:

$$\underline{\underline{A}}(\underline{x}).\underline{\alpha}(\underline{x}) = \underline{p}(\underline{0}) - \sum_{je\,\Omega^{FEM/MLS}} N_j^e(\underline{x}) \underline{p}(\underline{x}_j - \underline{x}) \tag{13}$$

4.2 Shape functions

Dirichlet boundary conditions are taken into account at the interface $\Omega^{FEM/MLS}$ (Fig.3.A) [6,11]. In the studied example, linear evolutions of N_j^e and ϕ_i^{MLS} shape functions, along x or y direction is at first evaluated. The line evaluation « a » (Fig.3) shows the generation of MLS shape functions for $1 \leq x \leq 5\ mm$. The appearance of the combination of shape functions N_j^e and ϕ_i^{MLS} as gradually as $0 \leq x < 1\ mm$ and $5 \leq x < 6\ mm$ is shown in Fig.3.B.

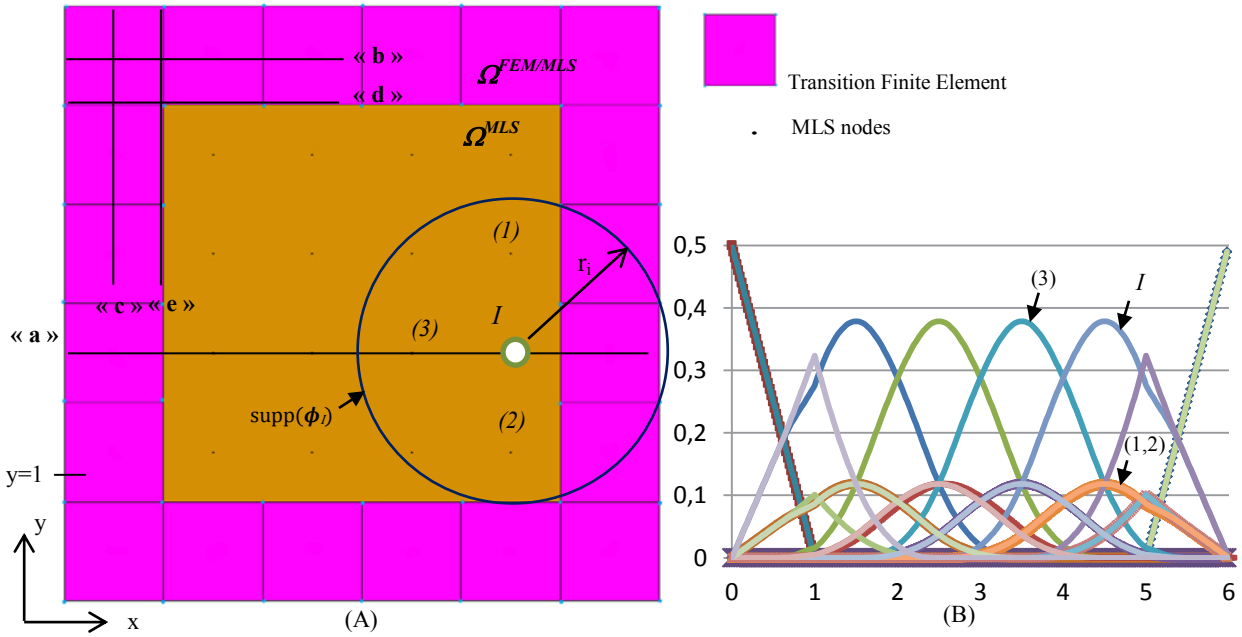

Figure 3: (A) Coupled FEM/MLS flat 2d example and radius of influence (B) Evolution of shape functions for a radius of influence r_i=2mm along « a » y=2.5mm

The curve generation shows the contribution of all nodes FEM and MLS for a given field of influence. The appearance of MLS shape functions depends on several parameters such as the order of consistency of the polynomial basis, the choice of weight functions $w(\underline{x}_i, \underline{x})$ and MLS nodes distribution in the Ω^{MLS} domain (Fig.3). MLS shape functions ϕ_i^{MLS}=0 when x=6mm (and by symmetry x = 0mm). Besides, ϕ_i^{MLS} (6, y) = 0 for all equal consistency between Ω^{MEF} and Ω^{MLS} domains is fulfilled. According to Huerta et al., MLS shape functions ϕ_i^{MLS} take care of the consistency of the approximation. In fact, MLS shape functions adapt their shape to recover the linear interpolation (Fig.3.B) in the interface domain $\Omega^{FEM/MLS}$.

Linear evolutions of N_j^e and ϕ_i^{MLS} shape functions, along x or y direction with $x \in [0\ 3]$ and $y \in [3\ 6]$ (Fig.4) are also outlined to estimate the shape function evolution along a well specific transition domain. Thus, The evaluation lines of « b » y = 5.5 mm along $x \in [0\ 3]$ (Fig.4.b) and « c » x = 0.5 along $y \in [3\ 6]$ (Fig.4.c) represent the shape functions curves at the corner transition zone $\Omega^{MEF/MLS}$. The evaluation along the limit edge between $\Omega^{MEF/MLS}$ and Ω^{MLS} « d» (y = 5mm) denotes the disappearance of FE shape functions N_j^e (Fig.4.d) and this gradually as the distance from the line « b » to Ω^{MLS} domain.

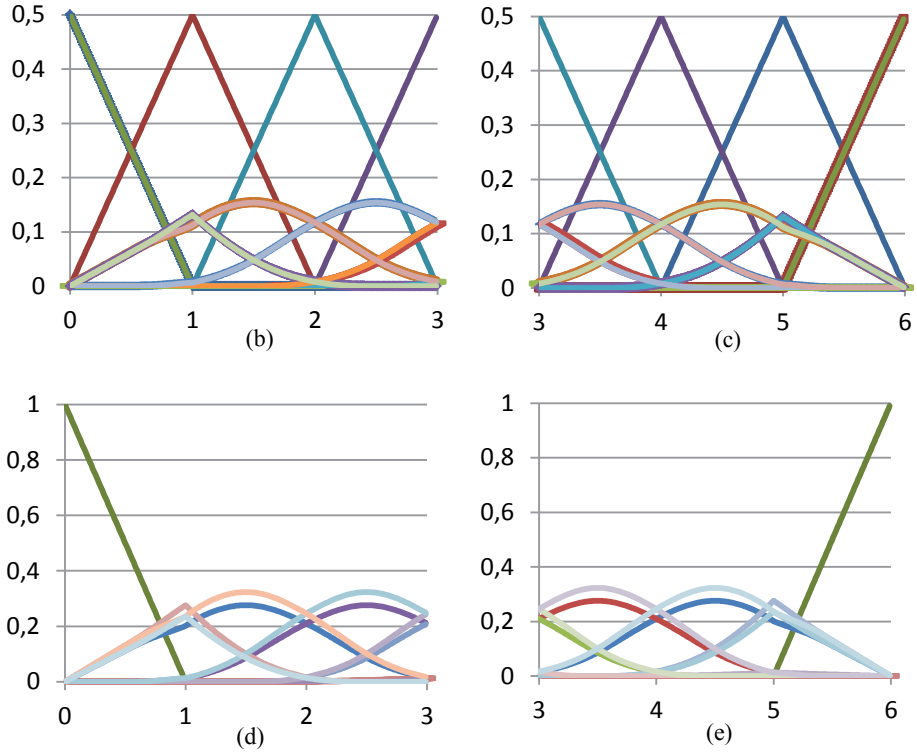

Figure 4: Evolution of shape functions along lines: (b) y=5.5mm along x (c) x=0.5mm along y (d) y=5mm along x (e) x=1mm along y

5 NUMERICAL IMPLEMENTATION

5.1 Smooth nodal conforming integration

A method of a regularized gradient nodal integration is developed to fulfill the problem of spatial integration of rational shape functions generated by MLS method. Only MLS nodes are used as integration points. Therefore, Ω^{MLS} field is generated by Voronoi cells. Each cell defines a domain of nodal integration Ω_L of the representative domain associated to the MLS node $"L"$ with x coordinates $\underline{x}_L$ (fig.5). The integration by Gauss-Legendre method is applied on the Ω^{FEM} domain because of its simplicity and robustness. For the stability of the integration scheme, a smoothing technique is proposed deformations by Chen et al. [5]. Thus, the modified strain tensor in the node $"L"$ is as bellow.

$$\tilde{\varepsilon}_{ij}^h(\underline{x}_L) = \frac{1}{2A_L}\int_{\Omega_L}\left(\frac{\partial u_i^h}{\partial x_j} + \frac{\partial u_j^h}{\partial x_i}\right) d\Omega = \frac{1}{2A_L}\int_{\Gamma_L}(u_i^h n_j + u_j^h n_i)d\Gamma \tag{14}$$

Γ_L is the boundary of the representative domain Ω_L of node $"L"$ which area is $\boldsymbol{A_L} = \int_{\Omega_L} \mathbf{d}\Omega$.

$$\underline{\tilde{\varepsilon}^h}(\underline{x}_L) = \sum_{I\in G_L} \underline{\underline{\tilde{B}_I}}(\underline{x}_L)\underline{\hat{u}_I} \tag{15}$$

Where G_L is a group of nodes in which their associated shape function supports cover node $"L"$. $\underline{\tilde{\varepsilon}^h}^T(\underline{x}_L) = [\tilde{\varepsilon}_{11}^h, \tilde{\varepsilon}_{22}^h, 2\tilde{\varepsilon}_{12}^h]$, $\underline{\hat{u}_I}^T = [\hat{u}_{1I}, \hat{u}_{2I}]$, $\underline{\underline{\tilde{B}_I}}$ is the stabilized gradient matrix used for

the nodal integration for the Ω^{MLS} domain (Eq.16) and G_L is the group of nodes *"I"* as $\underline{x}_L \in Supp(\phi_I)$ (Fig.5).

$$\underline{\underline{\tilde{B}_I}}(\underline{x}_L) = \begin{bmatrix} \tilde{b}_{I1}(\underline{x}_L) & 0 \\ 0 & \tilde{b}_{I2}(\underline{x}_L) \\ \tilde{b}_{I2}(\underline{x}_L) & \tilde{b}_{I1}(\underline{x}_L) \end{bmatrix}, \text{ Tel que } \tilde{b}_{Ii}(\underline{x}_L) = \frac{1}{A_L}\int_{\Gamma_L} \phi_I(\underline{x})\, n_i(\underline{x})\, d\Gamma \tag{16}$$

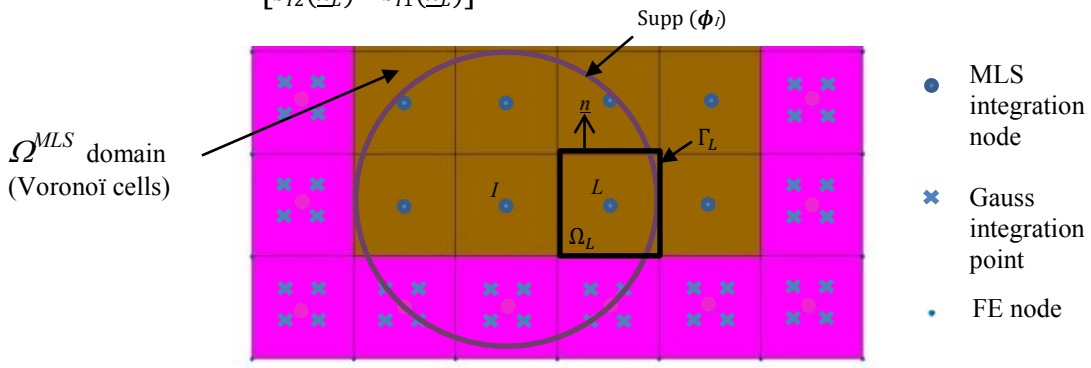

Figure 5: Voronoi cells for Ω^{MLS} and supp (ϕ_I) generation

Nodal evaluation components $\tilde{b}_{Ii}(\underline{x}_L)$ are calculated at nodal location $\underline{x}_L$ (Eq.16). A boundary integration of representative nodal domain is required; letting $\Gamma_L = \cup_{M=1}^{N_s} \Gamma_L{}^M$ as $\Gamma_L{}^M$ are the boundary segments of Γ_L, Ns the total number of segments and M = Ns+1 the node number of the Ω_L domain. A five Simpson rule for each segment of the representative nodal boundary $\Gamma_L{}^M$ is considered. The internal force vector reflecting mechanical equilibrium of the system is obtained from the following relationship:

$$\underline{F}^{int} = \underline{F}^{int}_{MEF} + \underline{F}^{int}_{MEF/MLS} + \underline{F}^{int}_{MLS} = \underline{F}^{int}_{MEF} + \sum_{L\in\Omega^{MLS}} \underline{\underline{\tilde{B}}}^T(\underline{x}_L).\underline{\tilde{\sigma}}\left(\underline{\tilde{\varepsilon}}(\underline{x}_L)\right) A_L \tag{17}$$

5.2 Numerical example

Tensile test of a flat 2D plane strain specimen is chosen to test the numerical methodology (Fig.6.a). The material behavior is governed by an elastoplastic model without hardening:

$$f(\underline{\sigma}) = \sqrt{\frac{3}{2}\underline{\sigma}^{dev} : \underline{\sigma}^{dev}} - \sigma_S \le 0 \tag{18}$$

Where $\underline{\sigma}$ is the Cauchy stress tensor, $\underline{\sigma}^{dev}$ the deviatoric part of the stress tensor and σ_S a yield stress value. The material parameters used for this example are: Young's modulus E=210 GPa, Poisson's ratio ν = 0.3 and σ_S = 500 MPa. Some boundaries conditions are imposed to represent the fixation of the specimen with the grips. Displacement boundary conditions are imposed at one extremity as in Fig.6.b. Abaqus® software was used at first to simulate the plastic deformation of the specimen, the FE specimen is meshed with CPE4R elements (1.5x1.5 mm^2 size). An implicit scheme resolution is used to solve equilibrium (see Fig.6.b). In Fig.6.c the same tensile test is used with our numerical FEM/MLS method is presented. The heads of the specimen are meshed with 2D FEM elements "assumed strain" which references are given in the following article [15]. The useful part of the specimen is

discretized with MLS nodes. Transition FEM/MLS and boundaries are discretized with transition elements FEM/MLS (pink area). Square weight functions with a radius of influence a = b = 2.5mm in order to assume an efficient MLS node number for $\underline{\underline{A}}$ matrix construction.

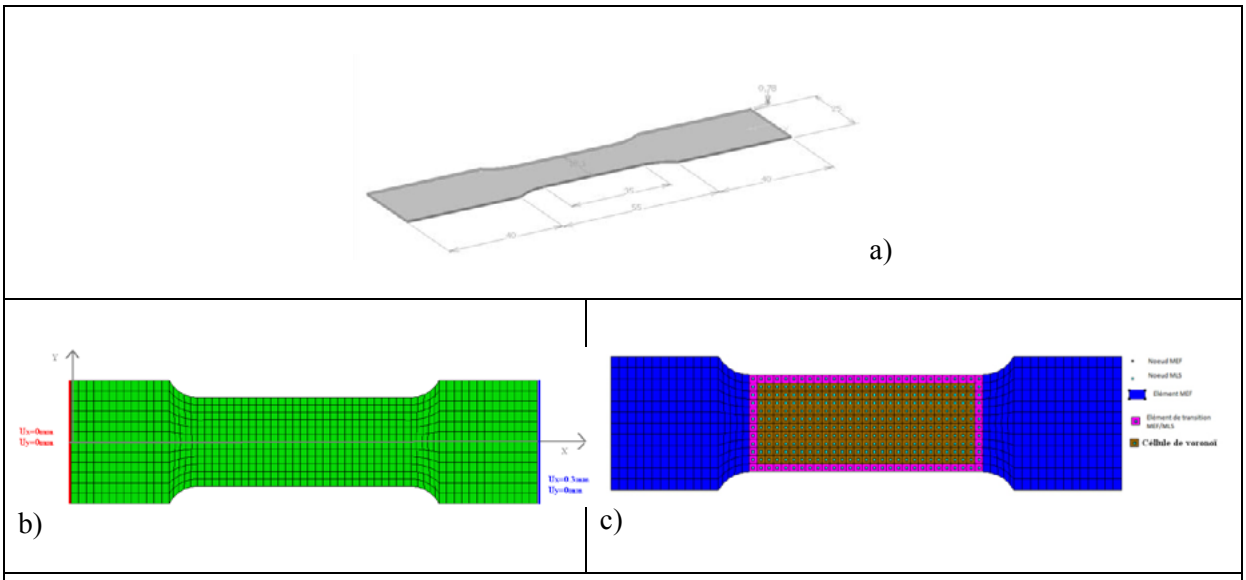

Figure 6: a) Plane specimen dimensions, b) Initial mesh of CPE4R elements + Dirichlet conditions, c) Ω^{MEF}, $\Omega^{MEF/MLS}$, Ω^{MLS} domains repartition and MLS node initial position.

After a maximum displacement of 0.3mm, displacement and stress distribution in the specimen for Abaqus® and numerical method based on coupled FEM/MLS are revealed below.

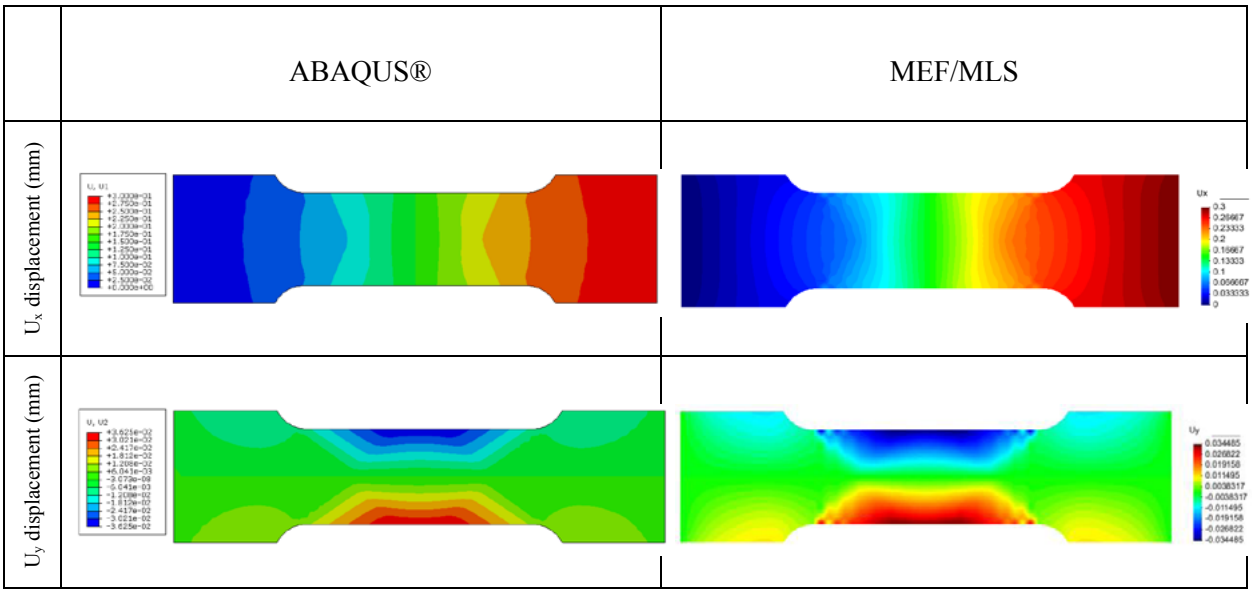

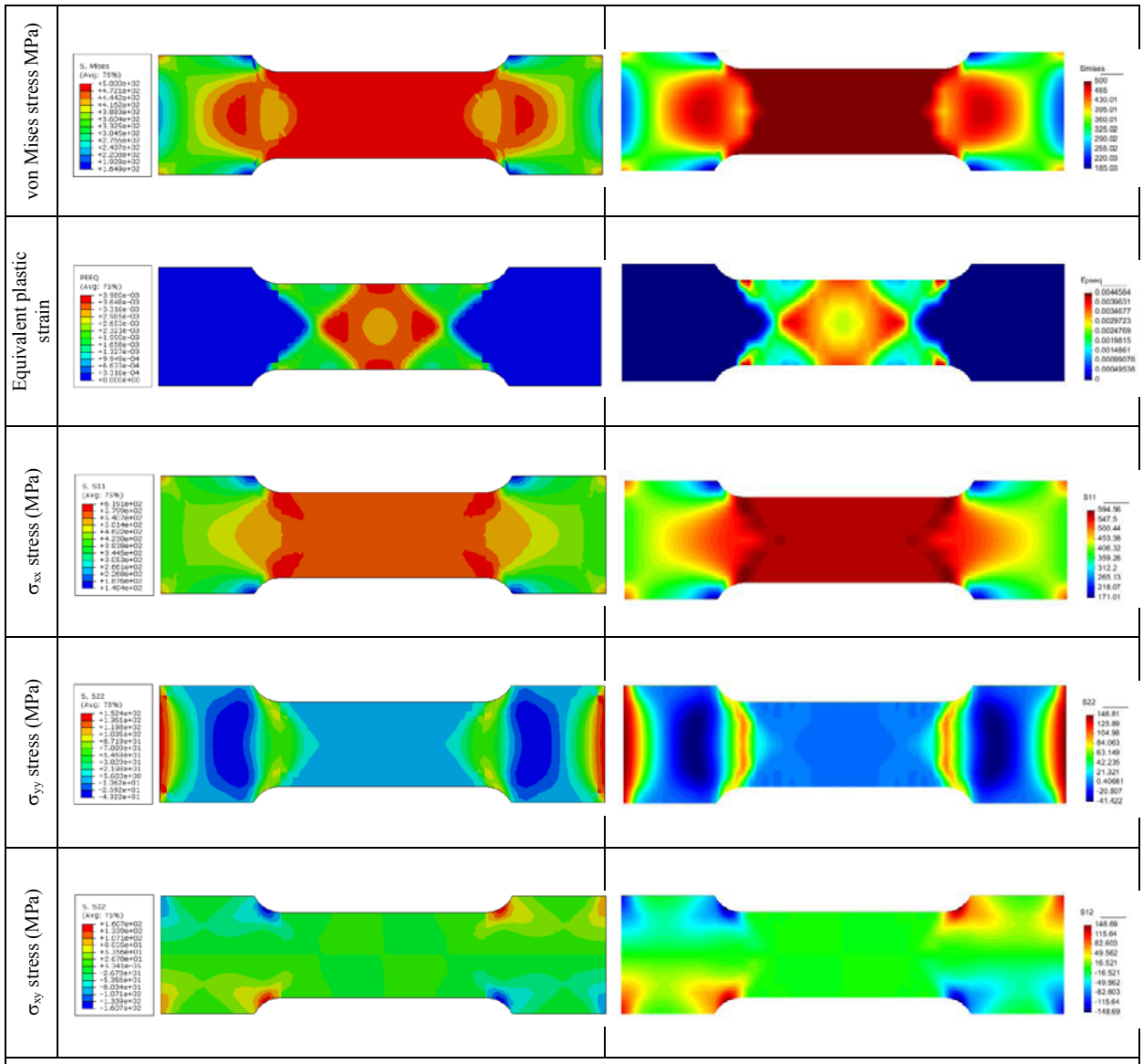

Figure 7: Numerical result comparison between Abaqus® software and the numerical method based on coupled FEM/MLS

Figure 7 shows that results in displacement are coherent. However, low amplitude oscillations appear in y components for FEM/MLS approach. These oscillations are probably generated by nodal integration revision and the occurrence of zero-energy mode. Von Mises and various stress tensor results are qualitatively similar for both approaches. Plastic flow is confined in the center of the specimen by both approaches; nevertheless, FEM/MLS method seems to have a better zone location for a proper and specific MLS node position.

The representation of the evolution of the stress xx is shown in Fig.8. We find that the two numerical approaches give equivalent results. However we visualize a difference in the transition zone FEM/MLS which is the highest stress gradient.

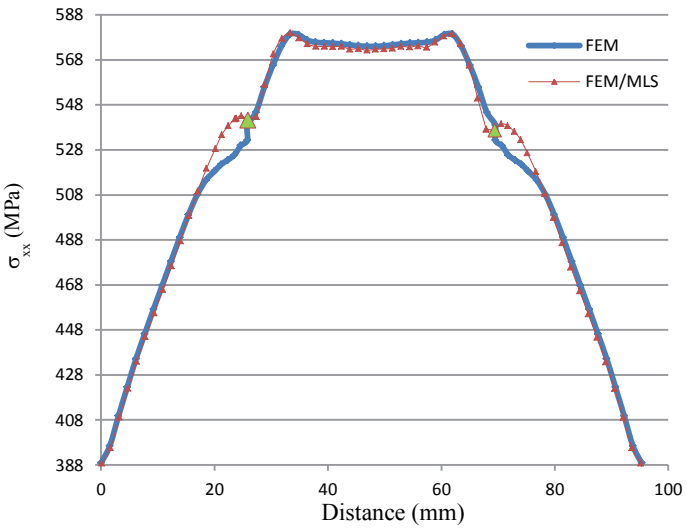

Figure 8: S11 stress evolution along the specimen length

6 CONCLUSIONS

A first validation of the coupled approach FEM/MLS is fulfilled. Results are hopeful, but some problems like zero-energy mode occurrence, nodal integration method sensitivity according to Voronoi cells construction, and weight functions radius sensitivity still remain. However, results give the possibility to set up some improvements to deal further with large deformation problems.

REFERENCES

[1] Belytschko T., Lu Y. and Gu L., Element-free Galerkin methods. *Int. J. Num. Meth. Eng.* (1994) **37**:229-256.

[2] Belytschko T., Organ D., and Krongauz Y., A coupled finite element – element-free Galerkin method. *Comput. Mech.* (1995) **17**:186–195.

[3] Breitkopf P., Rassineux A., Savignat J-M. and Villon P., Integration constraint in diffuse element method. *Computer Methods in Applied Mechanics and Engineering*, (2004) **193**:1203-1220.

[4] Breitkopf P., Rassineux A., Touzot G. and Villon P., Explicit form and efficient computation of MLS shape functions and their derivatives. *Int. J. Numer. Meth. Engng.* (2000) **48**:451–466.

[5] Chen J. S., Wu C. T., Yoon S. and You Y., A stabilized conforming nodal integration for Galerkin Meshfree methods, *Int. J. Num. Meth. Eng.* (2001) **50**:435–466.

[6] Fernandez-Mendez S. and Huerta A., Imposing essential boundary conditions in mesh-free methods. *Computer Methods in Applied Mechanics and Engineering*, (2004) **193:**1257-1275.

[7] Ghozzi Y., Labergere C. and P. Villon, Numerical simulation based on Meshless formulation. Application to 2D solid mechanics. *ASME ESDA. Engineering Systems Design and Analysis Conference* (11; 2012; France)
[8] Ghozzi Y., Labergere C. and Villon P., Numerical simulation based on MEF/MESHLESS coupling in axisymmetric elastoplasticity for 2D solid mechanics. *ESMC. European Solid Mechanics Conference* (8; 2012; Austria)
[9] Huerta A. and Fernandez-Mendez S., Enrichment and coupling of the finite element and meshless methods. *Int. J. Numer. Meth. Eng.* (2000) **48**:1615–1636.
[10] Huerta A., Fernandez-Mendez S. and Liu W. K., A comparison of two formulations to blend finite elements and mesh-free methods. *Comput. Meth. Appl. Mech. Eng.* (2004) **193**:1105–1117.
[11] Krongauz Y. and Belytschko T., Enforcement of essential boundary conditions in meshless approximations using finite elements. Comput. Methods Appl. *Mech. Engrg.* (1996) **131**:133–145.
[12] Labergere C., Rassineux A. and Saanouni K., 2D adaptive mesh methodology for the simulation of metal forming processes with damage, *International Journal of Material Forming* (2011) **3**:317-328.
[13] Most T. and Bucher C., New concepts for moving least squares: An interpolating non-singular weighting function and weighted nodal least squares. *Eng. Analysis with Boundary Elements* (2008) **32**:461–470.
[14] Nayroles B., Touzot G. and Villon P., Generalizing the finite element method: diffuse approximation and diffuse elements. *Comput. Mech.* (1992) **10**:307–318.
[15] Wang J., Chen J. and Li M., *A URI 4-node quadrilateral element by assumed strain method for non-linear problems*. Acta Mechanica Sineca, Vol. 20, (2004).